# How hot is the hot zone? Computational modelling clarifies the role of parietal and frontoparietal connectivity during anaesthetic-induced loss of consciousness

Riku Ihalainen[1*], Olivia Gosseries[2], Frederik Van de Steen[3], Federico Raimondo[2,4], Rajanikant Panda[2], Vincent Bonhomme[5,6], Daniele Marinazzo[3], Howard Bowman[1,7], Steven Laureys[2†], Srivas Chennu[1,8†]

[1] School of Computing, University of Kent, United Kingdom

[2] Coma Science Group, GIGA Consciousness, University and University Hospital of Liège, Liège, Belgium

[3] Department of Data Analysis, Faculty of Psychology and Educational Sciences, Ghent University, Belgium

[4] Institut du Cerveau et de la Moelle épinière, Paris, France.

[5] GIGA - Consciousness, Anesthesia and Intensive Care Medicine Laboratory, University and CHU University Hospital of Liège, Liège, Belgium

[6] University Department of Anesthesia and Intensive Care Medicine, CHR Citadelle and CHU Liege, Liège, Belgium

[7] School of Psychology, University of Birmingham, United Kingdom

[8] Department of Clinical Neurosciences, University of Cambridge, United Kingdom

[*] Corresponding author
Riku Ihalainen – rji4@kent.ac.uk

Medway Building, University of Kent
Chatham Maritime
Kent, ME4 4AG

[†] Both authors contributed equally

## Highlights

- Modelling shows that connectivity within hot zone tracks change of conscious state
- Separately, frontoparietal connections support maintenance of conscious state
- Strength of frontoparietal connections predicts conscious state in unseen data
- Both parietal hot zone and frontoparietal connectivity important for consciousness

## Abstract

In recent years, specific cortical networks have been proposed to be crucial for sustaining consciousness, including the posterior hot zone and frontoparietal resting state networks (RSN). Here, we computationally evaluate the relative contributions of three RSNs – the default mode network (DMN), the salience network (SAL), and the central executive network (CEN) – to consciousness and its loss during propofol anaesthesia. Specifically, we use dynamic causal modelling (DCM) of 10 minutes of high-density EEG recordings ($N$ = 10, 4 males) obtained during behavioural responsiveness, unconsciousness and post-anaesthetic recovery to characterise differences in effective connectivity within frontal areas, the posterior 'hot zone', frontoparietal connections, and between-RSN connections. We estimate – for the first time – a large DCM model (LAR) of resting EEG, combining the three RSNs into a rich club of interconnectivity. Consistent with the hot zone theory, our findings demonstrate reductions in inter-RSN connectivity in the parietal

cortex. Within the DMN itself, the strongest reductions are in feed-forward frontoparietal and parietal connections at the precuneus node. Within the SAL and CEN, loss of consciousness generates small increases in bidirectional connectivity. Using novel DCM leave-one-out cross-validation, we show that the most consistent out-of-sample predictions of the state of consciousness come from a key set of frontoparietal connections. This finding also generalises to unseen data collected during post-anaesthetic recovery. Our findings provide new, computational evidence for the importance of the posterior hot zone in explaining the loss of consciousness, highlighting also the distinct role of frontoparietal connectivity in underpinning conscious responsiveness, and consequently, suggest a dissociation between the mechanisms most prominently associated with explaining the contrast between conscious awareness and unconsciousness, and those maintaining consciousness.

**Keywords:** Anesthesia; Consciousness; EEG; Effective connectivity; Dynamic causal modeling

**Acknowledgements**

We gratefully acknowledge support from the University of Kent's High Performance Computing facility.

**Funding**

This work was supported by the UK Engineering and Physical Sciences Research Council (EP/P033199/1), Belgian National Funds for Scientific Research (FRS-FNRS), the University and University Hospital of Liege, the

Fund Generet, the King Baudouin Foundation, the AstraZeneca Foundation, the European Union's Horizon 2020 Framework Programme for Research and Innovation under the Specific Grant Agreement No. 945539 (Human Brain Project SGA3), DOCMA project (EU-H2020-MSCA–RISE–778234), the BIAL Foundation, the European Space Agency (ESA) and the Belgian Federal Science Policy Office (BELSPO) in the framework of the PRODEX Programme, the Center-TBI project (FP7-HEALTH- 602150), the Public Utility Foundation 'Université Européenne du Travail', "Fondazione Europea di Ricerca Biomedica", the Mind Science Foundation, the European Commission, and the Special Research Fund of Ghent University. O.G. is research associate and S.L. is research director at the F.R.S-FNRS.

**Declaration of interest:**

None.

**Significance Statement:**

Various connectivity studies have suggested multiple network-level mechanisms driving changes in the state of consciousness, such as the posterior hot zone, frontal-, and large-scale frontoparietal networks. Here, we computationally evaluate evidence for these mechanisms using dynamic causal modeling for resting EEG recorded before and during propofol-anaesthesia, and demonstrate that, particularly, connectivity in the posterior hot zone is impaired during propofol-induced unconsciousness. With a robust cross-validation paradigm, we show that connectivity in the large-scale frontoparietal networks can consistently predict the state of consciousness and further generalise these findings to an unseen state of recovery. These results suggest a dissociation between the mechanisms most prominently associated with explaining the contrast between conscious awareness and unconsciousness, and those maintaining consciousness.

# How hot is the hot zone? Computational modelling clarifies the role of parietal and frontoparietal connectivity during anaesthetic-induced loss of consciousness

## 1. Introduction

Several cortical network-level mechanisms have been proposed to explain human consciousness and its loss, of which two, in particular, have received an increasing amount of interest and evidence. On the one hand, empirical studies have suggested that the loss of consciousness (LOC)[1] is associated with disruptions of within- and between-network connectivity in cortical areas associated with large-scale frontoparietal networks (Bor & Seth, 2012; Laureys & Schiff, 2012). On the other, temporo-parieto-occipital areas – colloquially named as 'the posterior hot zone' – has been shown to be important in mediating changes in consciousness during sleep (Siclari et al., 2017; Lee et al., 2019), and in patients with brain damage (Vanhaudenhuyse et al., 2010; Wu et al., 2015).

[1] We acknowledge that anaesthetic-induced loss of consciousness (LOC) may actually be anaesthetic-induced loss of behavioural responsiveness (LOBR), as e.g. volitional mental imagery or dreaming may take place during the anaesthetic state. The participants were, however, asked afterwards if they had any recall of dreams etc., which they did not report. Thus, here, we follow the typical convention in anaesthesia-literature and refer to this state as LOC.

In this context, general anaesthetics are a powerful tool to investigate alterations in brain connectivity during changes in the state of consciousness (see Bonhomme et al., 2019 for a recent review). Indeed, several previous studies have utilised anaesthetic drugs in investigating brain dynamics in both functional and effective/directed connectivity studies and suggested multiple explanatory mechanisms of the LOC. Note that here, effective connectivity is defined following (Friston, 2011) and (Razi & Friston, 2016) as a causal influence (in a control theory sense) of one neural population over another and functional connectivity as undirected statistical dependencies between distinct neurophysiological events. Some of these studies have suggested a breakdown of thalamo-cortical connections and disrupted frontoparietal networks (Boveroux et al., 2010; Schrouff et al., 2011). Others have found disruptions in frontal areas (Guldenmund et al., 2016), diminished frontoparietal feedback connectivity (Lee et al., 2009; Lee, Ku et al., 2015), and increased frontoparietal connectivity (Barrett et al., 2012). To bring computational evidence to bear upon this discussion, we adopt one of the most commonly used methods for understanding effective connectivity, dynamic causal modeling (DCM; Friston, Harrison & Penny, 2003), to assess cortical network-level mechanisms involved in the LOC, and evaluate the evidence for the posterior hot zone.

There are relatively few studies assessing resting state effective connectivity with DCM during anaesthetic-induced unconsciousness, but a recent fMRI study identified impaired subcortico-cortical connectivity between globus pallidus and posterior cingulate (PCC) nodes, but no cortico-cortical modulations (Crone, Lutkenhoff, Bio, Laureys, & Monti, 2017). Boly et al. (2012) found a decrease in feedback connectivity from frontal (dorsal anterior

cingulate; dACC) to parietal (PCC) nodes. Both of these studies, however, evaluated relatively simple models in terms of cortical sources (excluding subcortical nodes), consisting of only two such nodes – an anterior and a posterior node. Consequently, they do not allow us to compare the role of the posterior hot zone to other potential cortical mechanisms underpinning consciousness.

Here, we address this gap by modelling changes in key resting state networks (RSN) - the default mode network (DMN), the salience network (SAL), and the central executive network (CEN), due to unconsciousness induced by propofol, a common clinical anaesthetic. We employ a novel methodological combination of DCM for resting EEG cross-spectral densities (CSD; Friston et al., 2012; Moran et al., 2009) and Parametric Empirical Bayes (PEB; Friston et al., 2016), to better estimate model parameters (and their distributions) and prune redundant connections. Within this framework, we invert - for the first time - a single large-scale model of EEG, consisting of 14 RSN nodes, in addition to the individual RSNs themselves (figure 1). This allows us to evaluate the role of different subgroups of intra- and inter-RSN connections in the modulation of consciousness. Further, we apply robust leave-one-subject-out-cross-validation (LOSOCV) on DCM model parameters, to evaluate hypotheses about whether specific sets of connections within and between frontal and parietal nodes are not only able to explain changes between states of consciousness, but also to predict the state of consciousness from unseen EEG data. Using this combination of computational modelling, cross-validation and hypothesis testing, we indicate the importance of the posterior hot zone in explaining the loss of consciousness, while highlighting also the

distinct role of frontoparietal connectivity in underpinning conscious responsiveness. Consequently, we demonstrate a dissociation between the mechanisms most prominently associated with explaining the contrast between conscious awareness and unconsciousness, and those maintaining consciousness.

# 2. Methods

## 2.1 Data acquisition and preprocessing

The data used in the present work were acquired from a previous propofol anaesthesia study, which describes the experimental design and data collection procedure in detail (Murphy et al., 2011). The study was approved by the Ethics Committee of the Faculty of Medicine of the University of Liège, and written consent was obtained from all the participants. None of the participants suffered from mental illness, drug addiction, asthma, motion sickness, nor had a history of mental illness or suffered from any previous problems with anaesthesia. The data consisted of 15 minutes of spontaneous, eyes-closed high-density EEG recordings (256 channels, EGI) from 10 participants (mean age 22 ± 2 years, 4 males) in four different states of consciousness: behavioural responsiveness, sedation (Ramsay scale score 3, slower responses to command), loss of consciousness with clinical unconsciousness (Ramsay scale score 5-6, no response to command), and recovery of consciousness (Ramsay, Savege, Simpson, & Goodwin, 1974). Note that for the recovery state, the data consisted of 9 datasets. Participants were considered to be fully awake if the response to

verbal command ('squeeze my hand') was clear and strong (Ramsay 2), and in LOC, if there was no response (Ramsay 5-6). The Ramsay scale verbal commands were repeated twice at each level of consciousness. Propofol was infused through an intravenous catheter placed into a vein of the right hand or forearm, and the propofol plasma and effect-site concentrations were estimated with 3.87 ± 1.39 mcg/mL average arterial blood concentration of propofol for LOC. Here, we only modelled data from the maximally different anaesthetic states, behavioural responsiveness and LOC, and used recovery as a test of DCM model generalisation. These data can be made available after signing a formal data-sharing agreement with the University of Liège.

Data from channels from the neck, cheeks, and forehead were discarded as they contributed most of the movement-related noise, leaving 173 channels on the scalp for the analysis. These 173 electrodes were co-registered to a template MRI mesh in MNI coordinates, and the volume conduction model of the head was based on the Boundary Element Method (BEM). The raw EEG signals were filtered from 0.5 – 45 Hz with additional line noise removal at 50 Hz using a notch filter. The recordings were then downsampled to 250 Hz, and abnormally noisy channels and epochs were identified by calculating their normalised variance, and then manually rejected or retained by visual inspection. Last, the data were then re-referenced using the average reference.

## 2.2 Dynamic causal modeling

For the DCM modelling of the high-density EEG data, the first 60 artefact-free 10-second epochs in wakeful behavioural responsiveness and LOC

were combined into one dataset with two anaesthetic states making up a total of 120 epochs per participant. The preprocessed data was imported in to SPM12 (Wellcome Trust Centre for Human Neuroimaging; www.fil.ion.ucl.ac.uk/spm/software/spm12).

To analyse effective connectivity within the brain's resting state networks, DCM for EEG cross-spectral densities (CSD) was applied (Friston et al., 2012; Moran et al., 2009). Briefly, with this method, the observed cross-spectral densities in the EEG data are explained by a generative model that combines a biologically plausible neural mass model with an electrophysiological forward model mapping the underlying neural states to the observed data. Each node in the proposed DCM models – that is, each electromagnetic source – consists of three neural subpopulations, each loosely associated with a specific cortical layer; pyramidal cells, inhibitory interneurons and spiny stellate cells (ERP model; Moran, Pinotsis & Friston, 2013). DCM does not simply estimate the activity at a particular source at a particular point in time – instead, the idea is to model the source activity over time, in terms of interacting inhibitory and excitatory populations of neurons.

The subpopulations within each node are connected to each other via *intrinsic* connections, while nodes are connected to each other via *extrinsic* connections. Three types of extrinsic connections are defined, each differing in terms of their origin and target layers/subpopulation: forward connections targeting spiny stellate cells in the granular layer, backward connections targeting pyramidal cells and inhibitory interneurons in both supra- and infragranular layers, and lateral connections targeting all subpopulations. This laminar specificity in the extrinsic cortical connections partly defines the

hierarchical organisation in the brain. Generally speaking, the backward connections are thought to have more inhibitory and largely modulatory effect in the nodes they target (top-down connections), while forward connections are viewed as having a strong driving effect (bottom-up; Salin & Bullier, 1995; Sherman & Guillery, 1998).

The dynamics of hidden states in each node are described by second-order differential equations which depend on both, the parametrised intrinsic and extrinsic connection strengths. This enables the computation of the linear mapping from the endogenous neuronal fluctuations to the EEG sensor spectral densities, and consequently, enables the modelling of differences in the spectra due to changes in the underlying neurophysiologically meaningful parameters describing, for example, the intrinsic and extrinsic connectivity of coupled neuronal populations (i.e. sources) and their physiology. Here, for straight-forward interpretability, we have focused on the changes in extrinsic connections as a result of changes in the state of consciousness. It should be noted that we did not fix any of the other parameters typically estimated by DCM using the ERP-model, rather, we estimated all our models using the default DCM setting (for further information about EEG DCM, see for example Friston et al., 2012; Kiebel, Garrido, Moran, & Friston, 2008; Moran, Kiebel et al., 2007; Moran et al., 2009). Nevertheless, from here on, we focus on the extrinsic connectivity parameters and their modulations referring to them as 'parameters'.

## 2.3 Model specification

Fitting a DCM model requires the specification of the anatomical locations of the nodes/sources a priori. Here, we modelled three canonical RSNs associated with consciousness (see for example Boly et al., 2008; Heine et al., 2012), namely the Default Mode Network (DMN), the Salience Network (SAL), and the Central Executive Network (CEN). In addition, we modelled a fourth large-scale network (LAR) combining all the nodes and connections in the three RSNs above, with additional inter-RSN connections motivated by structural connectivity (details below). The node locations of the three RSNs modelled here were taken from Razi et al. (2017) and are shown in figure 1 with their respective schematic representations (the node locations in figure 1 and the effective connectivity modulations in figures 4A, 5A, 6A, and 7A were visualized with the BrainNet Viewer (Xia, Wang, & He, 2013, http://www.nitrc.org/projects/bnv/). The MNI coordinates are listed in table 1. Coincidentally, these same data have been previously source localised to the same locations as some of the key nodes in the RSNs modelled here (Murphy et al., 2011). We treated each node as a patch on the cortical surface for constructing the forward model ('IMG' option in SPM12; Daunizeau, Kiebel, & Friston, 2009).

Nodes in the 3 RSNs were connected via forward, backward, and lateral connections as described in David et al. (2006, 2005). Thus, each node (in each RSN-model) were modelled as a point source with the neuronal activity being controlled by operations following the Jansen-Rit model (Jansen & Rit, 1995). Note that all our models were fully connected. In addition to preserving the connections within the nodes of the original 3 RSNs, in the LAR, we additionally hypothesised potential connections between the 3 RSNs. Previous

structural connectivity studies have identified a highly interconnected network of RSN hubs that seem to play a crucial role in integrating information in the brain, often termed the 'rich-club' (van den Heuvel & Sporns, 2011). Specifically, van den Heuvel and colleagues localised a number of these key-hubs to regions comprising of the precuneus, superior lateral parietal cortices, and superior frontal cortex, thus, to some extent overlapping with some of the key-nodes in our RSN models. Therefore, as a structurally-informed way to investigate the potential anaesthesia-induced modulations of effective connectivity between the 3 RSNs, we specified – in addition to the already-specified connections in our RSNs – bi-directional connections between PCC/precuneus and left/right superior parietal nodes (connecting DMN and CEN), and between PCC/precuneus and anterior cingulate cortex (connecting DMN and SAL).

These three different types of connections in each model were specified in what is referred in the DCM literature as the 'A-matrix'. In addition, to explicitly parameterise the effect of the session – i.e. the effect of the anaesthetic – on the connections, we allowed every connection to change (specified in the 'B-matrix').

**Table 1.** All the nodes and their corresponding MNI coordinates for the three resting state networks (adapted from Razi et al., 2017). The large model incorporated all these nodes as a single model.

| **Network** | **Coordinates (in mm)** |
|---|---|

| | | |
|---|---|---|
| **Default Mode Network** | | **x y z** |
| **1** Left lateral parietal | | -46 -66 30 |
| **2** Right lateral parietal | | 49 -63 33 |
| **3** Posterior cingulate/Precuneus | | 0 -52 7 |
| **4** Medial prefrontal | | -1 54 27 |
| | | |
| **Salience Network** | | |
| **1** Left lateral parietal | | -62 -45 30 |
| **2** Right lateral parietal | | 62 -45 30 |
| **3** Dorsal anterior cingulate | | 0 21 36 |
| **4** Left anterior PFC | | -35 45 30 |
| **5** Right anterior PFC | | 32 45 30 |
| | | |
| **Central Executive Network** | | |
| **1** Left superior parietal | | -50 -51 45 |
| **2** Right superior parietal | | 50 -51 45 |
| **3** Dorsal medial PFC | | 0 24 46 |
| **4** Left anterior PFC | | -44 45 0 |
| **5** Right anterior PFC | | 44 45 0 |

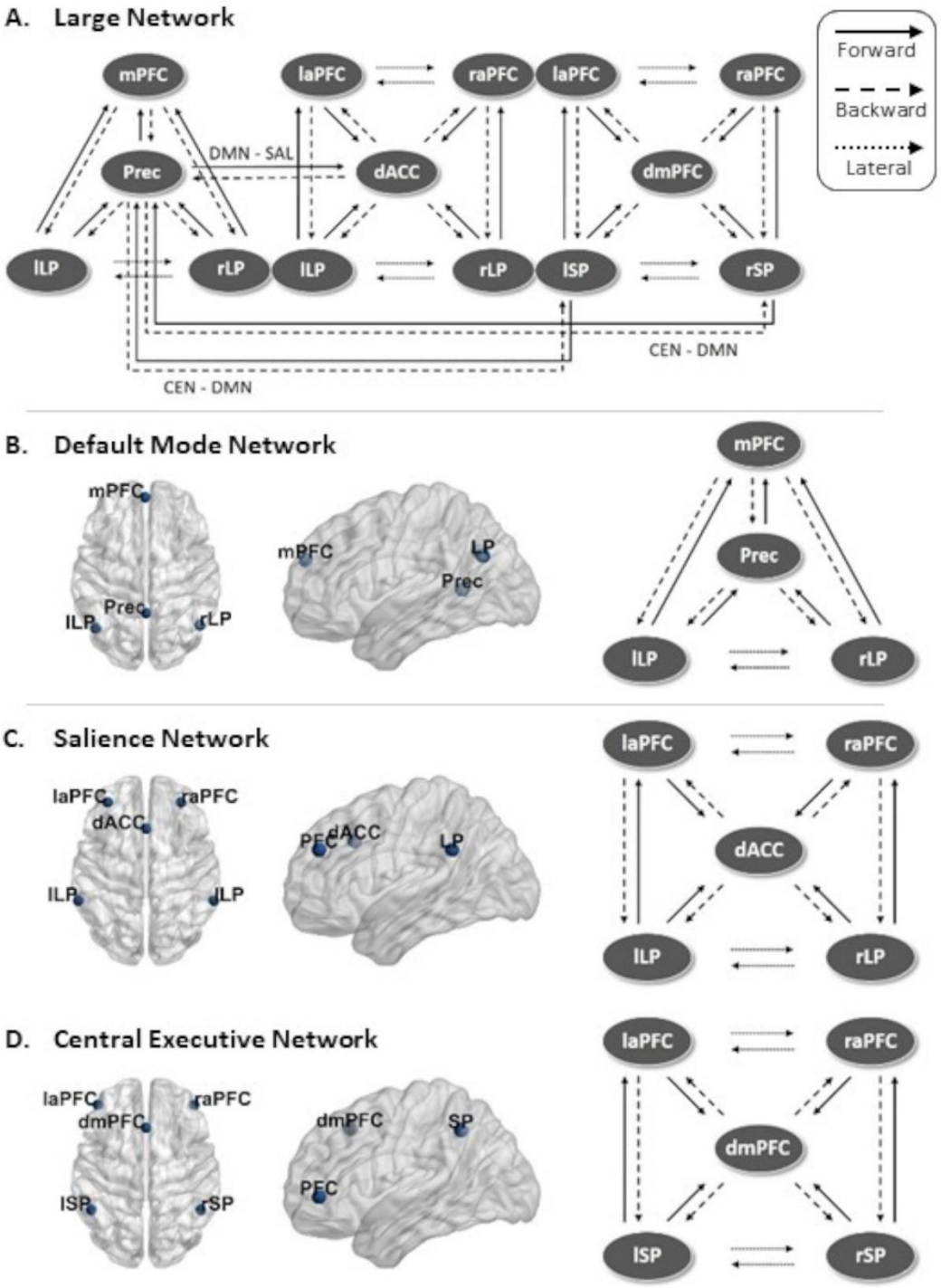


346

347 **Figure 1.** Full model schematics and node locations. **A.** Schematic view of the large DCM
348 model consisting of the 14 nodes and connections combining three RSNs. Inter-RSN
349 connections were specified between PCC/precuneus and bi-lateral superior parietal nodes,
350 and between PCC/precuneus and anterior cingulate cortex. **B-D.** Location of the nodes and
351 the schematic representation of the full model for DMN, SAL, and CEN, respectively.

352

353 **2.4 Model inversion**

354 In DCM, model inversion refers to fitting the models to best explain the
355 empirical data of each participant's dataset, and thereby inferring a full
356 probability density over the possible values of model parameters (with the
357 expected values and covariance). Here, we first modelled the effects of propofol
358 in terms of changes in connectivity that explained the differences in the
359 empirical data observed in LOC as compared to behavioural responsiveness
360 baseline (figure 3A). The EEG data used contained considerable peaks at the
361 alpha range (8-12 Hz), and the default parameter settings in DCM for CSD
362 failed to produce satisfactory fits to these peaks when inspected visually (see
363 van Wijk et al., 2018, *p.* 824). To address this issue, we doubled the number of
364 maximum iterations to 256 and estimated the models with two adjustments to
365 the hyperparameters: first, we set the shape of the neural innovations (i.e. the
366 baseline neuronal activity) to flat (-32) instead of the default mixture of white
367 and pink (1/f) components (Moran et al., 2009). Second, we increased the noise
368 precision value from 8 to 12 to bias the inversion process towards accuracy over
369 complexity (see Friston et al., 2012 and Moran et al., 2009 for a detailed
370 description of DCM for cross-spectral densities). In addition, for LAR the
371 number of spatial modes was increased to 14 instead of the default of 8. The
372 modes here refer to a reduction of the dimensionality of the data (done for
373 computational efficiency) by projecting the data onto the principal components
374 of the prior covariance, such that a maximum amount of information is retained
375 (David et al., 2006; Fastenrath, Friston, & Kiebel, 2009; Kiebel, Garrido,
376 Moran, & Friston, 2008).

These adjustments led to our full models (i.e. DMN, SAL, CEN, and LAR) converging with satisfactory fits (inspected visually) to the spectrum for 30/40 subject model instances (similar fits to what can be seen as the end result in figure 2). We then applied Bayesian Parameter Averaging (BPA) for each of the full models separately, averaging over the posteriors from the subject model instances that did converge and setting these averaged posteriors as new priors for the respective non-converged subject model instances. Estimating these subject model instances again with these BPA-derived priors produced satisfactory fits for all 10 remaining instances. Finally, we estimated all the full models again for all the participants with setting the posteriors from the earlier subject model estimations as updated priors, but this time with the neural innovations and noise precision set back to default settings. In doing so, all the models produced satisfactory fits with the default parameter settings for all of the participants (see figure 2).

To validate that the priors we used in the final inversion were suitable, we compared the group-level model evidence obtained with and without the adjusted noise levels. With all full models, the default hyperparameter settings with the updated priors generated better model evidence (difference in free energies for LAR, DMN, SAL, and CEN were +47260, +9440, +15700, and +660, respectively). To qualitatively assess the model fits, the observed and model-predicted cross-spectra were visually compared in each participant and judged to be sufficiently similar. To be sure about our conclusions, we also performed the PEB modelling (see below) leaving out the fitted subject model instances that produced the worst fits (1-2 per model); this had no notable influence on the interpretation of the results. The same approach was followed

when inverting the full models separately for individual states of consciousness (figure 3B); in addition to the full models, here the BPA was also restricted to the same state of consciousness. The model-predicted and original spectral densities averaged over participants are shown in figure 2A, B, C, and D for LAR, DMN, SAL, and CEN, respectively.

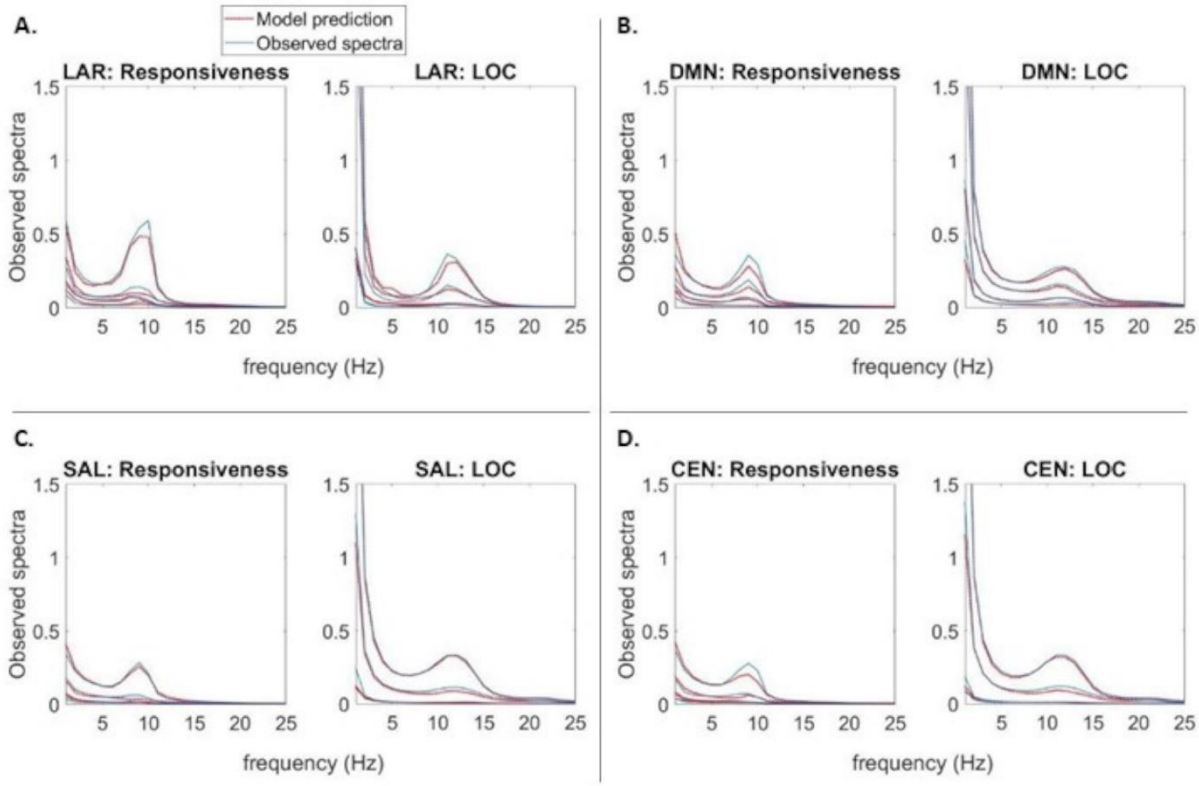


**Figure 2.** Average model fits. **A-D.** Subject-averaged power spectra of the observed EEG channel-space data, juxtaposed with that predicted by the fitted DCM models of each RSN, in normal behavioural responsiveness and LOC. Individual lines reflect spatial modes.

### 2.5 Parametric Empirical Bayes

In DCM, a variational Bayesian scheme called Variational Laplace is used to approximate the conditional or posterior density over the parameters

given by the model inversion process, by maximizing a lower bound (the negative free energy) on the log-evidence (Friston et al., 2007). The Parametric Empirical Bayes (PEB) framework is a relatively recent supplement to the DCM procedure used, for example, to infer the commonalities and differences across subjects (Friston et al., 2016). Briefly, the subject-specific parameters of interest (here, effective connectivity between nodes in a DCM model) are taken to the group-level and modelled using a General Linear Model (GLM), partitioning the between-subject variability into designed effects and unexplained random effects captured by the covariance component. The focus is on using Bayesian model reduction (BMR) – a particularly efficient form of Bayesian model selection (BMS) – to enable inversion of multiple models of a single dataset and a single hierarchical Bayesian model of multiple datasets that conveys both the estimated connection strengths and their uncertainty (posterior covariance). As such, it is argued that hypotheses about commonalities and differences across subjects can be tested with more precise parameter estimates than with traditional frequentist comparisons (Friston et al., 2016).

A particular advantage of PEB is that as part of the BMR process – when no strong a priori hypotheses about the model structure exist, as in the present study – a greedy search can be used to compare the negative free energies for the reduced models, iteratively discarding parameters that do not contribute to the free energy (originally 'post-hoc DCM analysis', Friston & Penny, 2011; Rosa, Friston & Penny, 2012). The procedure stops when discarding any parameters starts to decrease the negative free energy, returning the model that most effectively trades-off goodness of fit and model complexity in explaining the data. Last, a Bayesian Model Average (BMA) is calculated over the best

256 models weighted by their model evidence (from the final iteration of the greedy search). For each connection, a posterior probability for the connection being present vs. absent is calculated by comparing evidence from all the models in which the parameter is switched on versus all the models in which it is switched off. Here, we applied a threshold of >.99 posterior probability, in other words, connections with over .99 posterior probability were retained.

For the DCMs that were fitted to the contrast between two states of consciousness using the procedure described in the previous section, we used PEB for second-level comparisons and Bayesian model reduction to find the most parsimonious model that explained the contrast by pruning away redundant connections. The focus was explicitly on the group-level comparison of the connectivity modulations (B-matrix). The whole sequence of steps is summarized in figure 3A.

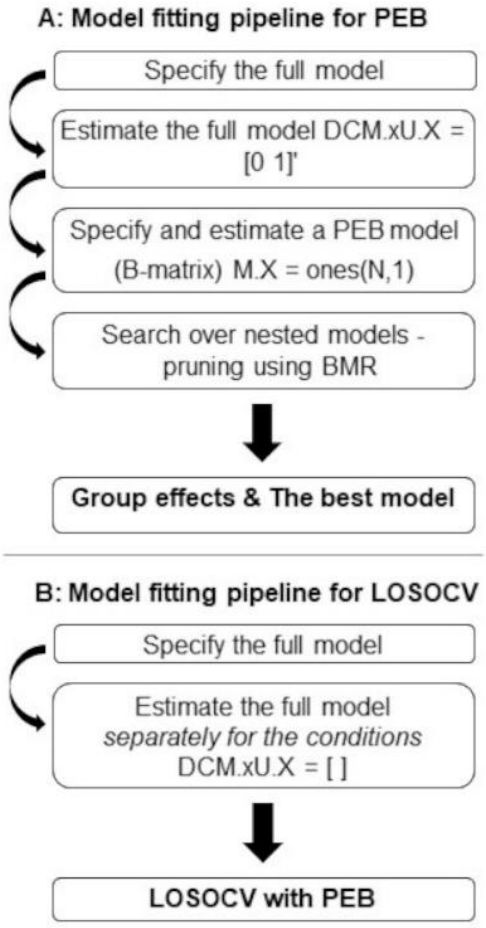


**Figure 3.** Modelling pipelines. **A.** The pipeline for inverting the DCM models in terms of changes in connectivity that explain the differences in the empirical data observed in LOC as compared to wakeful consciousness baseline. The DCM model inversion was followed by PEB modelling with BMR to find the most parsimonious model and the modulatory effects on the group-level effective connectivity. **B.** The pipeline for inverting the DCM models separately for individual states of consciousness. This was done as a prerequisite for the LOSOCV classification with PEB modelling.

### 2.6 Leave-one-out cross-validation paradigm

As a crucial form of validation of our modelling framework, we investigated which network connections are predictive of the state of

consciousness in unseen data. We adapted a standard approach in computational statistics, leave-one-subject-out cross-validation (LOSOCV; spm_dcm_loo.m). Here, we iteratively fitted a multivariate linear model (as described in detail in Friston et al., 2016) to provide the posterior predictive density over connectivity changes, which was then used to evaluate the posterior belief of the explanatory variable for the left-out participant: in the present case, the probability of the consciousness state-class membership.

To conduct LOSOCV analysis, the DCM models were now fitted to each state of consciousness separately, as shown in the procedure visualised in figure 3B. To cross-validate a fitted DCM model, both datasets from one participant were left-out each time *before* conducting PEB for the training data set, and the optimised empirical priors were then used to predict the state of consciousness (behavioural responsiveness/LOC) to which the datasets from the left-out participant belonged (see Friston et al., 2016 for details). This procedure, repeated for each participant, generated probabilities of state affiliation, which were used to calculate the Receiver Operating Characteristic (ROC) curves and Area Under the Curve (AUC) values with 95% point-wise confidence bounds across the cross-validation runs (see MATLAB `perfcurve`). In addition, the corresponding binary classification accuracy was calculated as the sum of true positives and true negatives divided by the sum of all assigned categories, i.e. (TP+TN) / (TP+TN+FP+FN), where TP = true positive, TN = true negative, FP = false positive, and FN = false negative.

We first estimated LOSOCV metrics for all connections in all models. Next, LOSOCV metrics of subsets of hypothesis-driven connections were tested; the connections preserved by BMR were divided into frontal, parietal,

492 frontoparietal, and between-RSN subsets, based on the anatomical location of
493 the connected nodes. The rationale was to investigate where in the brain the
494 most consistent inter-subject-level effects were located, in addition to the largest
495 effect sizes identified by the PEB analysis.

496 Finally, we extended our validation of the DCM models by introducing
497 a more difficult classification problem: we used the DCM parameters from
498 responsiveness and LOC for training, and then tested them on unseen data
499 collected during the post-drug recovery state of each subject (recovery state
500 prediction). Again during training, both datasets (behavioural
501 responsiveness/LOC) from one participant were left-out each time *before*
502 conducting PEB, and the optimised empirical priors were then used to predict
503 the state of consciousness to which the recovery-dataset from the left-out
504 participant belonged. We hypothesised that if our modelled effects are valid, it
505 should classify the recovery state as behavioural responsiveness rather than
506 LOC - even though recovery is not identical to normal wakeful responsiveness,
507 it is clearly closer to normal responsiveness than LOC. Here, we used recall -
508 as calculated by (true positive) / (true positive + false positive) - and mean
509 posterior probability for responsiveness to quantify classification performance.
510 The 95% CIs were calculated over the posterior probabilities using a simple
511 approximation for the unbiased sample standard deviation (Gurland & Tripathi,
512 1971).

513

514 # 3. Results

515

### 3.1 Dynamic causal modeling and parametric empirical Bayes

Our goal was to investigate the effective connectivity modulations caused by anaesthesia-induced loss of consciousness on three resting state networks together and separately. We modelled time-series recorded from two states of consciousness – wakeful behavioural responsiveness and loss of consciousness (LOC) – with DCM for CSD at a single-subject level, followed by PEB at the group-level. In doing so, we estimated the change in effective connectivity with RSNs during LOC, relative to behavioural responsiveness before anaesthesia. For the DMN, we estimated 12 inter-node connections, and for both SAL and CEN 16 connections. With LAR, in addition to including all the connections in each RSN, additional connections were specified to model the modulatory effects of anaesthesia on between-RSN connections, increasing the estimated inter-node connections to fifty.

Following the inversion of the second-level PEB model, a greedy search was implemented to prune away connections that did not contribute significantly to the free energy using BMR. This procedure was performed for LAR and for all the three resting state networks separately. The most parsimonious model (A) and estimated log scaling parameters (B) for LAR, DMN, SAL, and CEN are shown in figures 4-7, respectively. Here, we applied a threshold of >.99 for the posterior probability; in other words, connections that were pruned by BMR and connections with lower than .99 posterior probability with their respective log scaling parameter are faded out (figures 4B-7B).

Of the fifty connections in the large model (figure 4), five were pruned away by BMR. The results indicate that typically effective connectivity

decreased going from behavioural responsiveness to LOC between nodes in the DMN, with parietal connections showing consistent and large decreases. Similarly, between-RSN parietal connections linking DMN and CEN also decreased. Backward connections between the dACC and PCC/precuneus, linking the DMN and SAL, increased slightly. A clear majority of connections forming the SAL and CEN networks increased.

On inverting the DMN separately (figure 5), we found that no connections were pruned away by BMR. In other words, all of the effective connectivity in the DMN was modulated by the loss of consciousness. In particular, forward connectivity to and from PCC/precuneus largely decreased, whereas direct parietofrontal forward connectivity from lateral parietal cortices to the medial prefrontal cortex was increased. Backward connectivity between all the sources was increased.

In contrast, seven connections out of 16 were pruned away from the full SAL model when it was inverted separately (figure 6). These consisted of all but one lateral connections between both, the lateral prefrontal nodes and lateral parietal nodes, and all but one backward connection originating from the dACC. The strength of change in connectivity within the SAL was lower than in DMN, and all but one of the retained connections showed an increase in strength when losing consciousness.

When inverting the CEN separately, two connections were pruned away (figure 7). Most of the retained connections showed a small increase in strength, with the largest effects in frontoparietal connections from the dmPFC to the left

563 superior parietal cortex. Further, right hemisphere frontoparietal connections
564 showed more modulatory changes than left hemisphere connections.

565

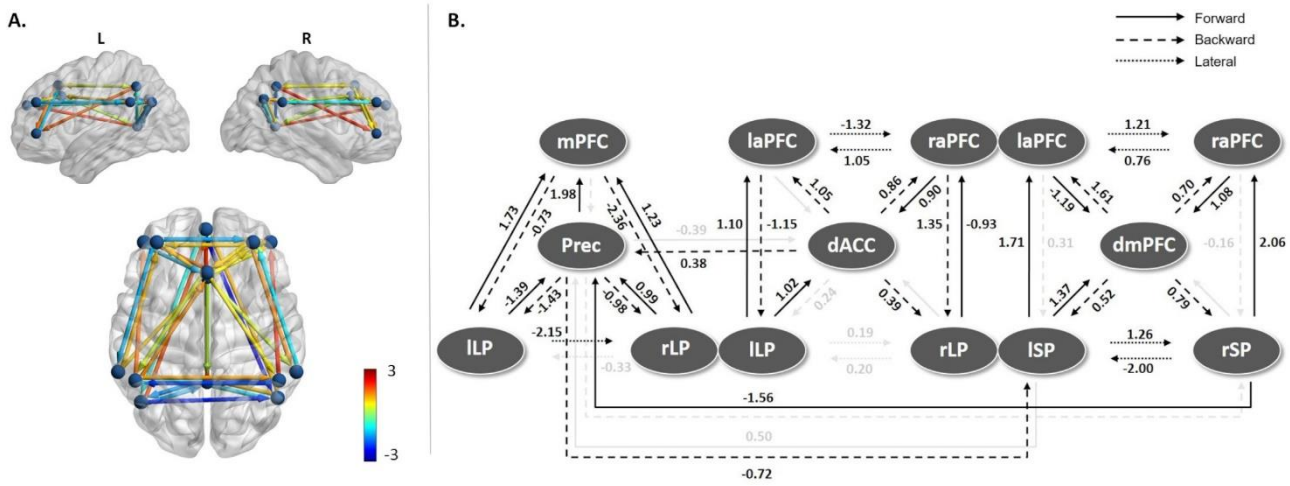


566

567 **Figure 4.** Estimated model parameters for LAR. **A.** Effective connectivity modulations on the
568 most parsimonious LAR model. 5 connections were pruned away by BMR and a further 8 had
569 lower than .99 posterior probability of being present. Colour shows modulation strength and
570 direction. **B.** The log scaling parameters for the connections in the large model after BMR and
571 BMA. Connections that were pruned by BMR and connections with lower than .99 posterior
572 probability with their respective log scaling parameter are faded out.

573

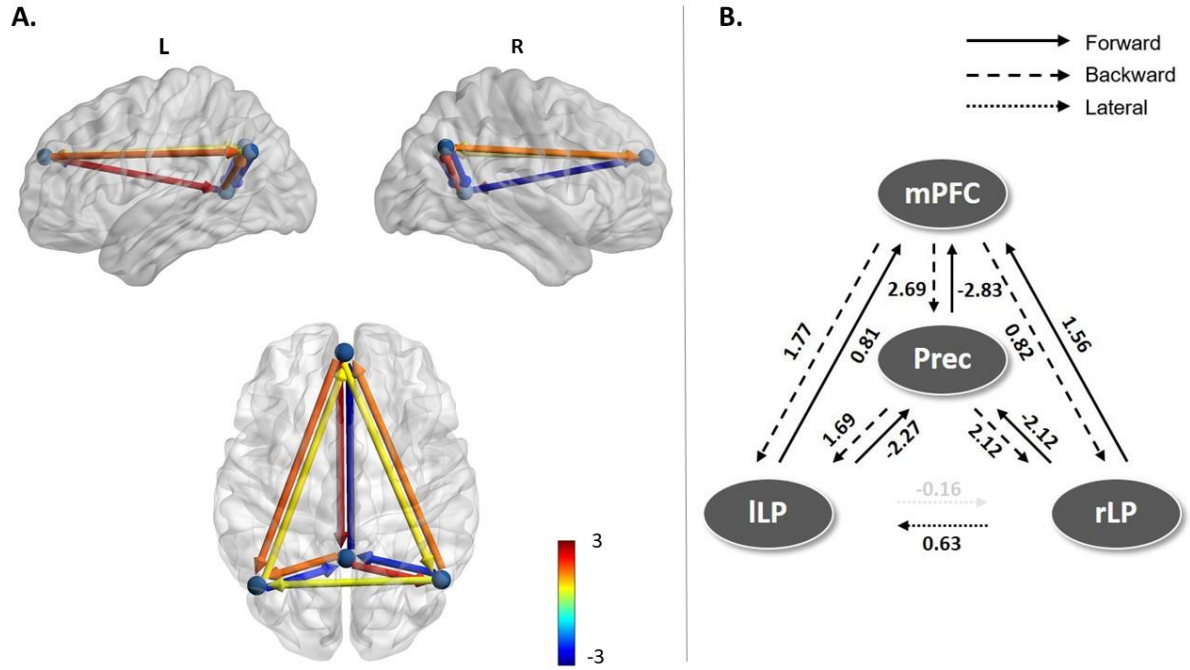


574

575 **Figure 5.** Estimated model parameters for DMN. **A.** Effective connectivity modulations on the
576 most parsimonious DMN model. Colour of connections show strength and direction of
577 modulation. None of the connections were pruned away, and only one connection had lower
578 than .99 posterior probability. **B.** The log scaling parameters for the connections in DMN after
579 BMR and BMA. The below-threshold posterior probability connection with its corresponding
580 log scaling parameter is faded out.

581

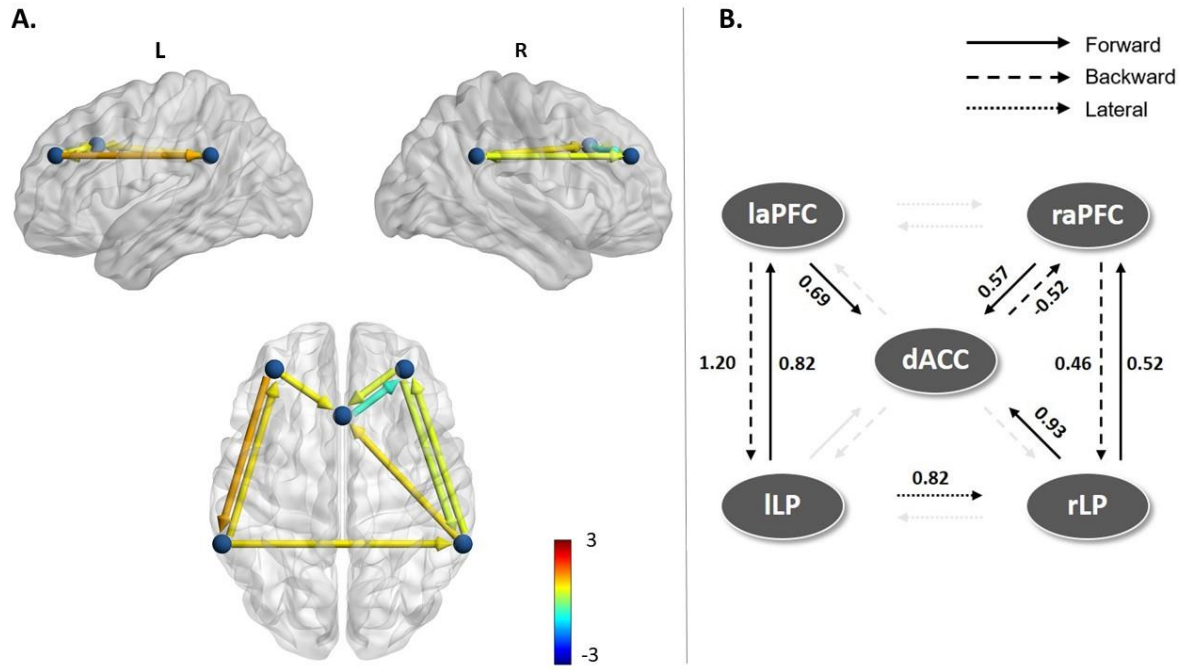


582

583 **Figure 6.** Estimated model parameters for SAL. **A.** Effective connectivity modulations on the
584 most parsimonious model for SAL. 7 connections were pruned by BMR. **B.** The log scaling
585 parameters for the connections in SAL. Several connections were pruned away (faded out).
586 The retained connections were almost all positive modulations, but smaller in strength than in
587 the DMN.

588

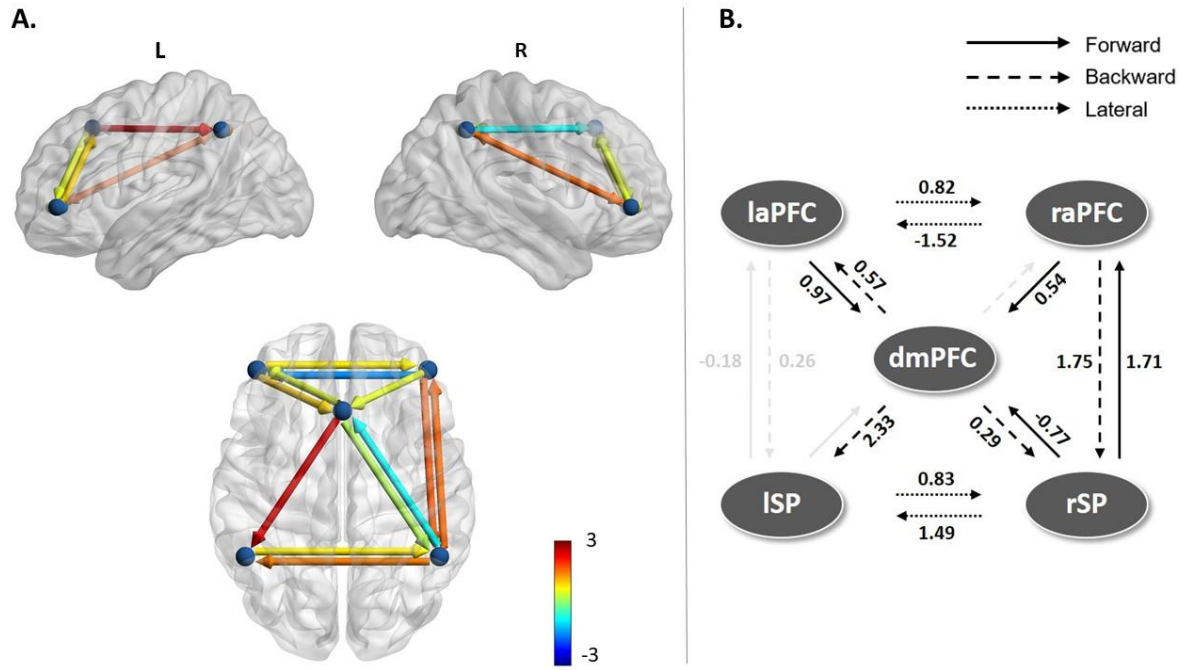


**Figure 7.** Estimated model parameters for CEN. **A.** Effective connectivity modulations on the most parsimonious model for CEN. 2 connections were redundant in addition to 2 connections having lower than .99 posterior probability for being switched on. **B.** The log scaling parameters for the connections in CEN. Pruned connections and low posterior probability connections with the corresponding log scaling parameters are faded out. Effects on the remaining connections were almost all positive modulations, with strengths in-between those observed in the SAL and DMN.

### 3.2 Leave-one-subject-out cross-validation

To conduct LOSOCV, the DCM models were inverted again, this time for each state of consciousness in each subject separately. With the states modelled separately, PEB was conducted repeatedly (on the training set in each cross-validation run) alongside LOSOCV analysis to generate AUC values (see Methods). The AUC/ROC values for all full models are shown in figure 8A,

and table 2 shows all tested AUC values with accuracy for all tested sets of connections. The results indicate that leave-one-subject-out cross-validated predictions based on the LAR and SAL models had accuracy significantly different from chance, i.e. with the lower bound of the 95% CI of the AUC above chance. However, for predictions based on the DMN and CEN, the lower bound of the 95% CI of the predictions did not exceed chance.

To understand whether specific connections within cortical brain networks were driving changes in consciousness, we evaluated the predictive power of four different hypothesis-driven subsets of connections – frontal, parietal, frontoparietal, or between-RSN – to predict the two states of consciousness in left-out subjects. As shown in figure 8B, frontoparietal connectivity in LAR, DMN, and SAL produced the best predictions of the state of consciousness with LOSOCV. Further, the posterior subset in the SAL performed statistically better than chance. None of the subsets in the CEN reached statistical significance.

Finally, the predictive power of these RSN connectivity subsets were tested in a more difficult classification problem: each model subset was trained on behavioural responsiveness and LOC, and then tested on the previously unseen 'recovery' state, the data which was collected after the participant regained consciousness. In figure 9A and B each data point represents one participant. Figure 9A shows the mean posterior probabilities of the recovery state being correctly classified as behavioural responsiveness when using all connections in a model as predictors. Figure 9B shows the same results for the frontal, parietal, frontoparietal, and between-RSN connections as predictors. When predicting with all connections, only classifications based on all

connections in LAR performed significantly better than chance. With the hypothesis-driven subsets of connections, frontoparietal connectivity within the DMN generalised best to the recovery state. Only one other subset – parietal connections in SAL – performed significantly better than chance, and almost as well as frontoparietal DMN connectivity (.82 vs. .79 posterior probability). All subsets with LAR performed statistically better than chance, however, with poor mean posterior probability values in comparison to DMN frontoparietal and SAL parietal connections. Table 2 shows the mean posterior probabilities and the corresponding recall values for all the tested connection sets and for all models. We verified that the predictive accuracy (of the unseen recovery state) was not driven by subject effects or bias, as evident in the individual posterior probabilities plotted in figures 9C and 9D.

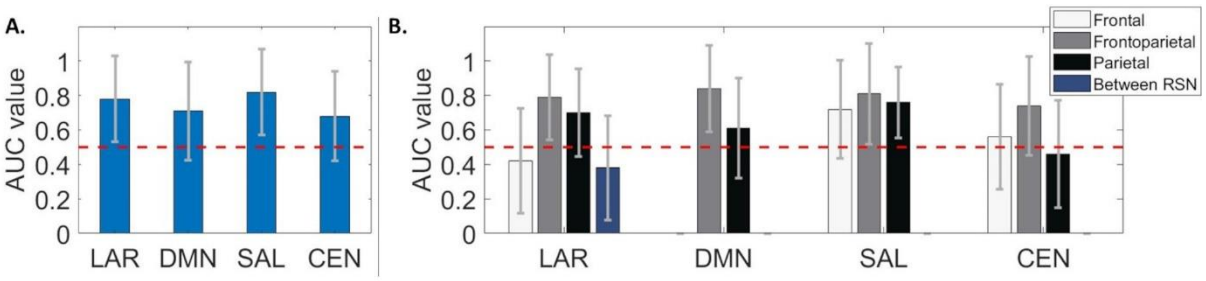


**Figure 8.** The AUC values for classifying the state of consciousness in LOSOCV paradigm. **A.** For the full models, only predictions based on LAR and SAL performed statistically better than chance (red dashed line), with classifications based on the connections in SAL reaching the overall best prediction. The error bars represent the 95% point-wise CI calculated using leave-one-out cross-validation for both A and B (MATLAB `perfcurve`). **B.** AUC values for hypothesis-driven connections for all models in LOSOCV paradigm. The DMN is missing frontal connections as it had only one anterior node. Best prediction performance was obtained

650 with frontoparietal connections in LAR, DMN, and SAL. Further, predictions based on
651 posterior SAL connections reached statistical significance.

652

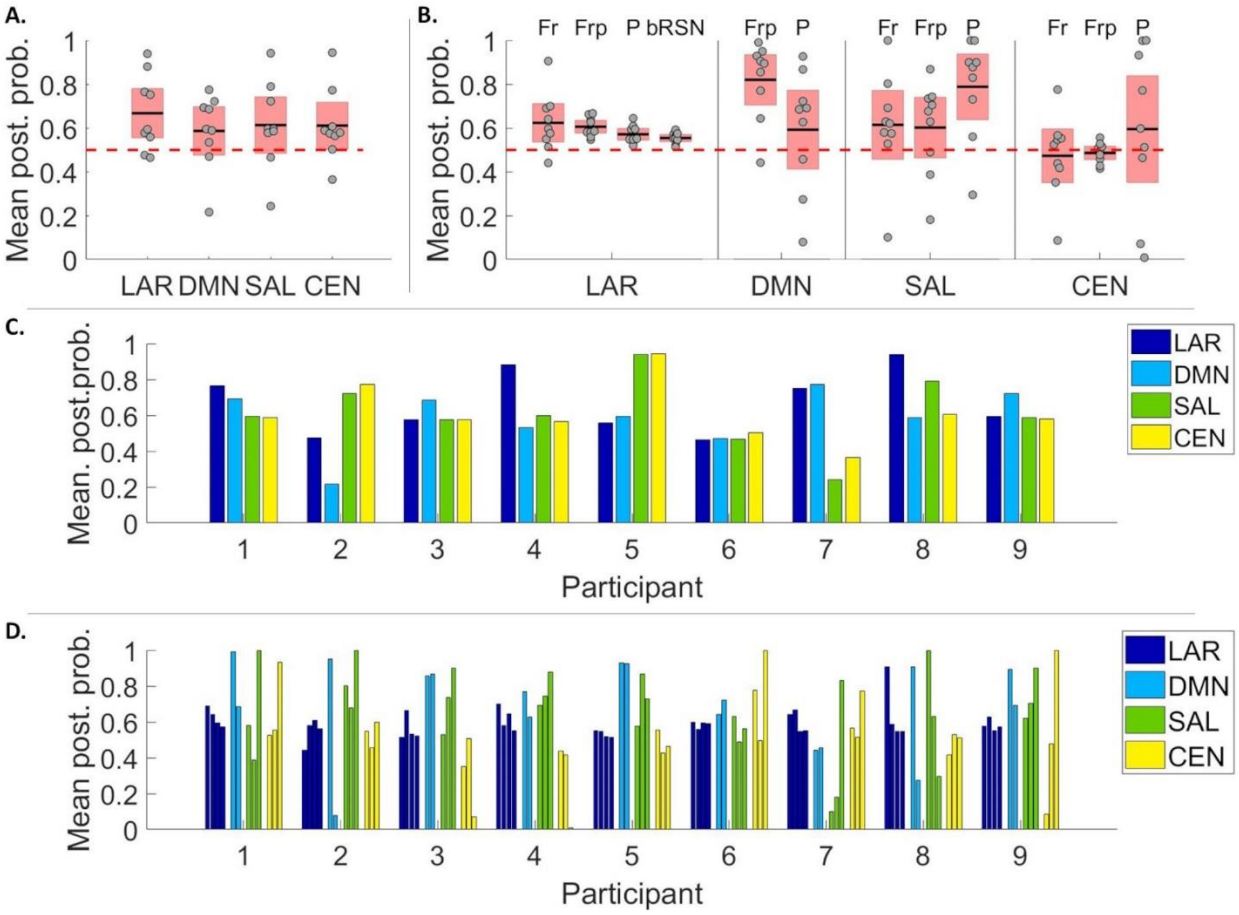


653

654 **Figure 9.** Mean posterior probabilities for prediction of recovery data. On panels A and B the
655 individual data points represent individual participants. **A.** Predictions based on all connections
656 in LAR performed better than chance (red dashed line). Data points representing participants
657 are laid over a 1.96 SEM (95% confidence interval over posterior probabilities) in red with the
658 black lines marking the mean. **B.** Mean posterior probabilities for hypothesis-driven connection
659 subsets of all models in the recovery state: top labels refer to frontal (Fr), frontoparietal (Frp),
660 parietal (P), and between-RSN (bRSN) connections. DMN frontoparietal connectivity had the
661 best performance across all sets and all models. Parietal connections in SAL performed
662 statistically better than chance but with lower posterior probability value in comparison to

DMN frontoparitetal connections. All subsets with LAR performed statistically better than chance, however, with poor posterior probability values in comparison to DMN frontoparietal and SAL parietal connections. **C-D.** Posterior probabilities predicted for individual datasets, based on all connections (C) and on hypothesis-driven subsets (D). In Panel D, the individual bars depict different connection subsets: frontal, frontoparietal, parietal, and between-RSN in LAR, frontoparietal and parietal in DMN, and frontal, frontoparietal, and parietal in SAL and CEN.

**Table 2.** AUC (accuracy) values calculated with LOSOCV, and mean posterior probabilities (recall) in the recovery state, for all connections, all hypothesis-driven connection subsets (frontal, parietal, frontoparietal, and between-RSN connections), and all models. No values are given if no such connection-subsets exist for the model. Accuracy/recall values were not calculated for connection subsets with performance close to chance (between 0.4 - 0.6). * indicates significance estimated at 95% confidence intervals in both AUC and posterior probability.

| **Model** | **Responsiveness/LOC** | **Recovery** |
|---|---|---|
| | **AUC (Accuracy)** | **Mean PP. (Recall)** |
| | **All connections** | **All connections** |
| Large network | 0.78 (0.80)* | 0.67 (0.78)* |
| Default mode network | 0.71 (0.70) | 0.59 (--) |
| Salience network | 0.82 (0.80)* | 0.61 (0.78) |
| Central executive network | 0.68 (0.70) | 0.61 (0.89) |

| | **Frontal** | **Parietal** | **Frontal** | **Parietal** |
|---|---|---|---|---|
| Large network | 0.42 (--) | 0.70 (0.65) | 0.62 (0.89)* | 0.57 (--)* |
| Default mode network | -- | 0.61 (.65) | -- | 0.59 (--) |
| Salience network | 0.72 (0.65) | 0.76 (0.65)* | 0.61 (.89) | 0.79 (0.89)* |
| Central executive network | 0.56 (--) | 0.46 (--) | 0.47 (--) | 0.60 (--) |

| | **Frontoparietal** | **BRSN** | **Frontoparietal** | **BRSN** |
|---|---|---|---|---|
| Large network | 0.79 (0.80)* | 0.38 (0.55) | 0.61 (1.00)* | 0.55 (--)* |
| Default mode network | 0.84 (0.85)* | -- | 0.82 (0.89)* | -- |
| Salience network | 0.81 (0.75)* | -- | 0.60 (--) | -- |
| Central executive network | 0.75 (0.70) | -- | 0.49 (--) | -- |

# 4. Discussion

We computationally evaluated the evidence for the posterior hot zone theory of consciousness by modelling the relative contributions of three resting state networks (DMN, SAL, and CEN) for propofol-induced LOC. Using the recently introduced PEB framework, we characterised modulations in effective connectivity accompanying the loss of consciousness within and between these key RSNs. We found a selective breakdown of posterior parietal and medial feedforward frontoparietal connectivity within the DMN, and of parietal inter-network connectivity linking DMN and CEN. These results contribute to the

current understanding of anaesthetic-induced LOC, and more generally to the discussion of whether the neural correlates of consciousness have an anterior contribution (Del Cul, Dehaene, Reyes, Bravo, & Slachevsky, 2009), are predominantly frontoparietal (Bor & Seth, 2012; Chennu et al., 2014; Chennu, O'Connor, Adapa, Menon, & Bekinschtein, 2016; Laureys & Schiff, 2012), or posterior (Koch et al., 2016; Koch et al., 2016b; Siclari et al., 2017).

We used a novel DCM-based cross-validation to establish the predictive validity of our models, addressing an issue commonly present in DCM studies, including previous consciousness-related DCM studies - that the best model identified by BMS is only the best model among the models tested. Significant generalisation performance with cross-validation increases the level of confidence we can ascribe to our results. This analysis highlighted that frontoparietal effective connectivity consistently generated accurate predictions of individual states of consciousness. Furthermore, we demonstrated generalisation of this predictive power by showing that effective frontoparietal connectivity within the DMN and parietal connectivity within the SAL predicted the state of consciousness in unseen data from the post-anaesthetic recovery state.

With the large model combining all 3 RSNs, we observed consistent and wide-spread decreases in connectivity between posterior DMN nodes and between parietal connections linking DMN and CEN (figure 4). With the individual RSNs, we observed a selective breakdown of the DMN, specifically, decreases in feedforward connectivity to and from PCC/precuneus (figure 5). It is worth highlighting that most decreases in effective connectivity - both when the RSNs were modelled individually and as one large network - were between

nodes located within the posterior hot zone, and related specifically to PCC/precuneus – a key structure in the hot zone (Koch et al., 2016; Siclari et al., 2017). In other words, the network-level breakdown characterising the difference between behavioural responsiveness and LOC was mostly located within the parietal hot zone.

In the SAL and CEN networks, when fitted on their own, several connections were pruned away by BMR, with small increases in the majority of preserved connections; ¼ of the connections in CEN and almost half of the connections in SAL (7 out of 16) were pruned, in contrast to the DMN in which no connections were pruned (figures 6 and 7). The same pattern was present, although to a smaller degree, when the three RSNs were estimated together (LAR): fewest of the connections pruned were in the DMN, when compared with the SAL and CEN networks. This highlights the relative importance of the DMN over the SAL and CEN in explaining differences between states of consciousness and is consistent with the previous evidence from disorders of consciousness (Crone et al., 2011; Fernández-Espejo et al., 2012; Laureys, 2005; Laureys et al., 1999), anaesthesia (Boveroux et al., 2010), and sleep (Horovitz et al., 2009).

It is important to note, however, that there are multiple possible approaches to parameter estimation in DCM, both at the individual and at the group-level. The joint estimation method we chose utilises BMR and PEB. An alternative would be a step-by-step approach, which uses individually-estimated RSN posteriors as fixed priors when fitting the LAR, thereby reducing the number of free parameters. The joint estimation method hence enables us to fit comparatively larger models, but potentially with a risk of a more complex free

energy landscape (Litvak et al., 2019). Due to these modelling choices, we have limited our granularity of our inference to models and cortical regions within them, instead of interpreting the posterior densities of all possible fitted model parameters. The fact that we were able to demonstrate out-of-sample generalisation using our fitted models gave us confidence that the methodology was valid.

Keeping the above in mind, we did find that PCC/precuneus-related feedforward connectivity in the DMN is impaired during LOC. This is in contrast to two previous DCM studies of propofol anaesthesia, which have suggested either selective impairments in frontoparietal feedback connectivity from dACC to PCC (Boly et al., 2012), or subcortico-cortical modulations from globus pallidus to PCC (Crone et al., 2017). However, there are major methodological differences between the present study and the previous two that could explain these different results. Firstly, the examined model space was different. Secondly, both previous studies used models with only two cortical nodes summarising activity of frontal and parietal regions. They did not implement a wide search over a large model space using BMR and instead focused on evaluating a small number of hypothesis-specific models. We adopted a broader approach to model formulation and evaluation. In doing so, we expand upon these previous results by suggesting a selective breakdown of PCC/precuneus-related forward connectivity within the DMN. Our results differed from Boly et al. (2012) even when the direct connections between dACC and PCC/precuneus were modelled (in LAR) – we found an increase in feedback connectivity from dACC to PCC/precuneus and a small, low probability decrease in feed-forward connectivity. Our results are, however, in

line with previous studies showing increased frontoparietal connectivity with partial directed coherence (Maksimow et al., 2014) and with Granger Causality (Barrett et al., 2012; Nicolaou, Hourris, Alexandrou, & Georgiou, 2012) during anaesthesia.

It is noteworthy that impaired feedforward connectivity has been suggested to be the main modulation caused by propofol-anaesthesia in a recent DCM study with TMS-evoked potentials by Sanders et al. (2018). Their models consisted of 6 cortical sources (bilateral inferior occipital gyrus (IOG), bilateral dorsolateral PFC, and bilateral superior parietal lobule (SPL). They found predominantly impaired feedforward connectivity from right IOG to right SPL (specifically with theta/alpha-gamma coupling). Although they suggested that resting state activity was driven by feedback connectivity, while induced responses were driven by feedforward connectivity, it may be that restricting modulations to just two free parameters (connections) in the cortex simplifies the effects of propofol-induced LOC to the degree that they differ from estimations of more complex models.

Finally, the observed *increase* in effective connectivity between specific nodes (especially front-to-back) has been suggested previously to be due to the drug-specific effects of propofol rather than changes in states of consciousness (Långsjö et al., 2012; Maksimow et al., 2014). Hence, it may be that the relatively uniform increases in connectivity in the SAL and CEN, and the increased feedback connectivity in the DMN, were specific to propofol.

While the results of the LOSOCV cross-validation should be interpreted with caution given the limited number of participants in our study, the results indicated that, when using all connections, the above-chance prediction

performance of conscious state was only obtained with LAR and SAL, with the latter performing the best (figure 8A). With smaller, hypothesis-driven subsets, we found that the frontoparietal connections provided consistently the most accurate predictions in all models except the CEN (figure 8B). When predicting the unseen state of recovery (figure 9B), frontoparietal DMN connections performed the best, followed by parietal connections in SAL. It is worth highlighting that the frontoparietal DMN and parietal SAL connections predict the state correctly, even when the state actually differs from the true training state; recovery differs from normal wakeful responsiveness not only behaviourally, but also in terms of the residual propofol in the blood. However, the participants are conscious and responsive, and thus, recovery is considered as a state clearly closer to normal wakeful responsiveness than LOC.

Taken together, our prediction results highlighted an important role for frontoparietal connections. This is perhaps not surprising, as wakeful awareness is known to recruit the DMN (Raichle & Snyder, 2007); maintaining a state of conscious responsiveness requires an interaction between the posterior hot zone (the role of which is highlighted when modelling the *change* between states) and frontal areas, mediated by the frontoparietal connections. Previous literature has suggested dynamic changes in connectivity between brain networks during cognitive control (Cocchi, Zalesky, Fornito, & Mattingley, 2013; Leech, Braga, & Sharp, 2012) and anaesthetic-induced loss of consciousness (Luppi et al. 2019). The importance of frontoparietal connections in the present study when predicting states of behavioural responsiveness – a state of higher integration than LOC – is consistent with the notion that conscious, behavioural responsiveness requires a brain-wide "global workspace" supported by the

frontoparietal network (Baars, 1997; Dehaene & Changeux, 2011; Dehaene, Changeux & Christen, 2011; Mashour, Roelfsema, Changeux, & Dehaene, 2020). Hence, it is perhaps no surprise that the role of frontoparietal connections became prominent when we predicted individual states of consciousness rather than the contrast between them.

A number of previous studies have suggested a pivotal role of subcortical structures in transitions to unconsciousness (e.g. Baker et al., 2014; Liu et al., 2013; White & Alkire, 2003). Crone et al. (2017) reported a breakdown of connectivity between the globus pallidus and posterior cingulate cortex connectivity during LOC, followed by a reversal at recovery. It remains a possibility that the effective connectivity modulations found in the present study – especially in relation to the PCC/precuneus - are driven by subcortical structures that we did not model here, given the limitations of scalp EEG signals (Goldenholz et al., 2009). It might be worthwhile to further investigate the effects of LOC with fMRI DCMs, including large-scale models combining cortical and subcortical nodes with PEB with BMR to conduct a wider exploration of the model space.

In addition to the modelling being limited only to cortico-cortical connections, some of our results are arguably propofol-specific; for example, very different alterations have been observed between propofol and ketamine (Driesen et al., 2013; Sarasso et al., 2015). Hence, it may be that modelling the cortical effects of other anaesthetic agents would lead to very different sets of results. Further, we have modelled the effects using DCM and the standard ERP neuronal model, rather than modelling frameworks designed to capture more fine-grained properties of the EEG spectrum during anaesthesia (see for

example Bojak & Liley, 2005; Hutt & Longtin, 2010). DCM and the ERP neuronal model were chosen primarily in order to produce results that could be compared with the prior DCM work on modelling consciousness. Furthermore, we aimed to model consciousness at the network level, rather than at the level of the known molecular effects of propofol, e.g., prolongation of inhibitory post-synaptic potential time constants, that are known to take place within individual cortical and sub-cortical sources. A valuable future direction would be to investigate the predictive power of such effects and the extent to which they may drive the modulations in extrinsic connectivity. This could be done, for example, by using the LFP model or the Canonical Microcircuits model which are better suited for estimating the intrinsic connectivity and the molecular effects within the sources (Bastos et al., 2012; Moran et al., 2007). Lastly, as we tested only a pre-specified model space, the limitations imposed by this scope might have missed important mechanisms of conscious awareness not modelled here.

Notwithstanding these points, our results highlight a selective breakdown of inter- and intra-RSN effective connectivity in the parietal cortex, reinforcing the role of the posterior hot zone for human consciousness. However, modulations of frontoparietal connections were consistent enough to predict states in unseen data, demonstrating their causal role in maintaining behavioural responsiveness.

# References

Baars, B. J. (1997). In the theatre of consciousness. Global Workspace Theory, a rigorous scientific theory of consciousness. *Journal of Consciousness Studies*, *4*(4), 292–309. https://doi.org/10.1093/acprof:oso/9780195102659.001.1

Baker, R., Gent, T. C., Yang, Q., Parker, S., Vyssotski, A. L., Wisden, W., … Franks, N. P. (2014). Altered activity in the central medial thalamus precedes changes in the neocortex during transitions into both sleep and propofol anesthesia. *Journal of Neuroscience*, *34*(40), 13326–13335. https://doi.org/10.1523/JNEUROSCI.1519-14.2014

Barrett, A. B., Murphy, M., Bruno, M. A., Noirhomme, Q., Boly, M., Laureys, S., & Seth, A. K. (2012). Granger causality analysis of steady-state electroencephalographic signals during propofol-induced anaesthesia. *PLoS ONE*, *7*(1). https://doi.org/10.1371/journal.pone.0029072

Bastos, A. M., Usrey, W. M., Adams, R. A., Mangun, G. R., Fries, P., & Friston, K. J. (2012). Canonical Microcircuits for Predictive Coding. *Neuron*, *76*(4), 695–711. https://doi.org/10.1016/j.neuron.2012.10.038

Bojak, I., & Liley, D. T. J. (2005). Modeling the effects of anesthesia on the electroencephalogram. *Physical Review E - Statistical, Nonlinear, and Soft Matter Physics*, *71*(4), 1–22. https://doi.org/10.1103/PhysRevE.71.041902

Boly, M., Moran, R., Murphy, M., Boveroux, P., Bruno, M.-A., Noirhomme, Q., … Friston, K. (2012). Connectivity Changes Underlying Spectral EEG Changes during Propofol-Induced Loss of Consciousness. *Journal of Neuroscience*, *32*(20), 7082–7090. https://doi.org/10.1523/JNEUROSCI.3769-11.2012

Boly, M., Phillips, L., Tshibanda, A. Vanhaudenhuyse, M. Schabus, D., Dang-Vu, T. T., Moonen, G., Hustinx, R., … Laureys, S. (2008). Intrinsic Brain Activity in Altered States of Consciousness: How Conscious Is the Default Mode of Brain Function? *Annals of the New York Academy of Sciences, 1129,* 119–129. https://doi.org/10.1196/annals.1417.015.Intrinsic

Bonhomme, V., Staquet, C., Montupil, J., Defresne, A., Kirsch, M., Martial, C., … Gosseries, O. (2019). General Anesthesia: A Probe to Explore Consciousness. *Frontiers in Systems Neuroscience*, *13*(August). https://doi.org/10.3389/fnsys.2019.00036

Bor, D., & Seth, A. K. (2012). Consciousness and the prefrontal parietal network: Insights from attention, working memory, and chunking. *Frontiers in Psychology*, *3*(MAR), 1–14. https://doi.org/10.3389/fpsyg.2012.00063

Boveroux, P., Vanhaudenhuyse, A., Bruno, M.-A., Noirhomme, Q., Lauwick, S., Luxen, A., … Boly, M. (2010). Breakdown of within- and between-network Resting State during Propofol-induced Loss of Consciousness. *Anesthesiology*, *113*(5), 1038–1053.

Chennu, S., Finoia, P., Kamau, E., Allanson, J., Williams, G. B., Monti, M. M., … Bekinschtein, T. A. (2014). Spectral Signatures of Reorganised Brain Networks in Disorders of Consciousness. *PLoS Computational Biology*, *10*(10). https://doi.org/10.1371/journal.pcbi.1003887

Chennu, S., O'Connor, S., Adapa, R., Menon, D. K., & Bekinschtein, T. A. (2016). Brain Connectivity Dissociates Responsiveness from Drug Exposure during Propofol-Induced Transitions of Consciousness. *PLoS Computational Biology*, *12*(1), 1–17. https://doi.org/10.1371/journal.pcbi.1004669

Cocchi, L., Zalesky, A., Fornito, A., & Mattingley, J. B. (2013). Dynamic cooperation and competition between brain systems during cognitive control. *Trends in Cognitive*

*Sciences*, *17*(10), 493–501. https://doi.org/10.1016/j.tics.2013.08.006

Crone, J. S., Ladurner, G., Höller, Y., Golaszewski, S., Trinka, E., & Kronbichler, M. (2011). Deactivation of the default mode network as a marker of impaired consciousness: An fmri study. *PLoS ONE*, *6*(10). https://doi.org/10.1371/journal.pone.0026373

Crone, J. S., Lutkenhoff, E. S., Bio, B. J., Laureys, S., & Monti, M. M. (2017). Testing proposed neuronal models of effective connectivity within the cortico-basal gangliathalamo-cortical loop during loss of consciousness. *Cerebral Cortex*, *27*(4), 2727–2738. https://doi.org/10.1093/cercor/bhw112

Daunizeau, J., Kiebel, S. J., & Friston, K. J. (2009). Dynamic causal modelling of distributed electromagnetic responses. *NeuroImage*, *47*(2), 590–601. https://doi.org/10.1016/j.neuroimage.2009.04.062

David, O., Harrison, L., & Friston, K. J. (2005). Modelling event-related responses in the brain. *NeuroImage*, *25*(3), 756–770. https://doi.org/10.1016/j.neuroimage.2004.12.030

David, O., Kiebel, S. J., Harrison, L. M., Mattout, J., Kilner, J. M., & Friston, K. J. (2006). Dynamic causal modeling of evoked responses in EEG and MEG. *NeuroImage*, *30*(4), 1255–1272. https://doi.org/10.1016/j.neuroimage.2005.10.045

Dehaene, S., Changeux, J.-P., & Christen, Y. (2011). The Global Neuronal Workspace Model of Conscious Access: From Neuronal Architectures to Clinical Applications. *Research and Perspectives in Neurosciences*, *18*, 55–84. https://doi.org/10.1007/978-3-642-18015-6

Dehaene, S., & Changeux, J. P. (2011). Experimental and Theoretical Approaches to Conscious Processing. *Neuron*, *70*(2), 200–227. https://doi.org/10.1016/j.neuron.2011.03.018

951 Del Cul, A., Dehaene, S., Reyes, P., Bravo, E., & Slachevsky, A. (2009). Causal role of
952 prefrontal cortex in the threshold for access to consciousness. *Brain*, *132*(9), 2531–2540.
953 https://doi.org/10.1093/brain/awp111

954 Driesen, N. R., McCarthy, G., Bhagwagar, Z., Bloch, M., Calhoun, V., D'Souza, D. C., …
955 Krystal, J. H. (2013). Relationship of resting brain hyperconnectivity and schizophrenia-
956 like symptoms produced by the NMDA receptor antagonist ketamine in humans.
957 *Molecular Psychiatry*, *18*(11), 1199–1204. https://doi.org/10.1038/mp.2012.194

958 Fastenrath, M., Friston, K. J., & Kiebel, S. J. (2009). Dynamical causal modelling for
959 M/EEG: Spatial and temporal symmetry constraints. *NeuroImage*, *44*(1), 154–163.
960 https://doi.org/10.1016/j.neuroimage.2008.07.041

961 Fernández-Espejo, D., Soddu, A., Cruse, D., Palacios, E. M., Junque, C., Vanhaudenhuyse,
962 A., … Owen, A. M. (2012). A role for the default mode network in the bases of
963 disorders of consciousness. *Annals of Neurology*, *72*(3), 335–343.
964 https://doi.org/10.1002/ana.23635

965 Friston, K. J., Bastos, A., Litvak, V., Stephan, K. E., Fries, P., & Moran, R. J. (2012). DCM
966 for complex-valued data: Cross-spectra, coherence and phase-delays. *NeuroImage*,
967 *59*(1), 439–455. https://doi.org/10.1016/j.neuroimage.2011.07.048

968 Friston, K. J., Harrison, L., & Penny, W. (2003). Dynamic causal modelling. *NeuroImage*,
969 *19*(4), 1273–1302. https://doi.org/10.1016/S1053-8119(03)00202-7

970 Friston, K., Mattout, J., Trujillo-Barreto, N., Ashburner, J., & Penny, W. (2007). Variational
971 free energy and the Laplace approximation. *NeuroImage*, *34*(1), 220–234.
972 https://doi.org/10.1016/j.neuroimage.2006.08.035

973 Friston, K., & Penny, W. (2011). Post hoc Bayesian model selection. *NeuroImage*, *56*(4),

2089–2099. https://doi.org/10.1016/j.neuroimage.2011.03.062

Friston, Karl J. (2011). Functional and Effective Connectivity: A Review. *Brain Connectivity*, *1*(1), 13–36. https://doi.org/10.1089/brain.2011.0008

Friston, Karl J., Litvak, V., Oswal, A., Razi, A., Stephan, K. E., Van Wijk, B. C. M., … Zeidman, P. (2016). Bayesian model reduction and empirical Bayes for group (DCM) studies. *NeuroImage*, *128*, 413–431. https://doi.org/10.1016/j.neuroimage.2015.11.015

Goldenholz, D. M., Ahlfors, S. P., Hämäläinen, M. S., Sharon, D., Ishitobi, M., Vaina, L. M., & Stufflebeam, S. M. (2009). Mapping the signal-to-noise-ratios of cortical sources in magnetoencephalography and electroencephalography. *Human Brain Mapping*, *30*(4), 1077–1086. https://doi.org/10.1002/hbm.20571

Guldenmund, P., Gantner, I. S., Baquero, K., Das, T., Demertzi, A., Boveroux, P., … Soddu, A. (2016). Propofol-Induced Frontal Cortex Disconnection: A Study of Resting-State Networks, Total Brain Connectivity, and Mean BOLD Signal Oscillation Frequencies. *Brain Connectivity*, *6*(3), 225–237. https://doi.org/10.1089/brain.2015.0369

Gurland, J., & Tripathi, R. C. (1971). A simple approximation for unbiased estimation of the standard deviation. *American Statistician*, *25*(4), 30–32. https://doi.org/10.1080/00031305.1971.10477279

Heine, L., Soddu, A., Gómez, F., Vanhaudenhuyse, A., Tshibanda, L., Thonnard, M., … Demertzi, A. (2012). Resting state networks and consciousness Alterations of multiple resting state network connectivity in physiological, pharmacological, and pathological consciousness states. *Frontiers in Psychology*, *3*(AUG), 1–12. https://doi.org/10.3389/fpsyg.2012.00295

Horovitz, S. G., Braun, A. R., Carr, W. S., Picchioni, D., Balkin, T. J., Fukunaga, M., &

997 Duyn, J. H. (2009). Decoupling of the brain's default mode network during deep sleep.
998 *Proceedings of the National Academy of Sciences*, *106*(27), 11376–11381.
999 https://doi.org/10.1073/pnas.0901435106

1000 Hutt, A., & Longtin, A. (2010). Effects of the anesthetic agent propofol on neural
1001 populations. *Cognitive Neurodynamics*, *4*(1), 37–59. https://doi.org/10.1007/s11571-
1002 009-9092-2

1003 Jansen, B. H., & Rit, V. G. (1995). Electroencephalogram and visual evoked potential
1004 generation in a mathematical model of coupled cortical columns. *Biological*
1005 *Cybernetics*, *73*(4), 357–366. https://doi.org/10.1007/BF00199471

1006 Kiebel, S. J., Garrido, M. I., Moran, R. J., & Friston, K. J. (2008). Dynamic causal modelling
1007 for EEG and MEG. *Cognitive Neurodynamics*, *2*(2), 121–136.
1008 https://doi.org/10.1007/s11571-008-9038-0

1009 Koch, C., Massimini, M., Boly, M., & Tononi, G. (2016a). Neural correlates of
1010 consciousness: Progress and problems. *Nature Reviews Neuroscience*, *17*(5), 307–321.
1011 https://doi.org/10.1038/nrn.2016.22

1012 Koch, C., Massimini, M., Boly, M., & Tononi, G. (2016b). Posterior and anterior cortex —
1013 where is the difference that makes the difference? *Nature Reviews Neuroscience*, *17*(10),
1014 666–666. https://doi.org/10.1038/nrn.2016.105

1015 Långsjö, J. W., Alkire, M. T., Kaskinoro, K., Hayama, H., Maksimow, A., Kaisti, K. K., …
1016 Scheinin, H. (2012). Returning from oblivion: Imaging the neural core of consciousness.
1017 *Journal of Neuroscience*, *32*(14), 4935–4943.
1018 https://doi.org/10.1523/JNEUROSCI.4962-11.2012

1019 Laureys, S., Goldman, S., Phillips, C., Van Bogaert, P., Aerts, J., Luxen, A., … Maquet, P.

(1999). Impaired effective cortical connectivity in vegetative state: Preliminary investigation using PET. *NeuroImage*, *9*(4), 377–382. https://doi.org/10.1006/nimg.1998.0414

Laureys, Steven. (2005). The neural correlate of (un)awareness: Lessons from the vegetative state. *Trends in Cognitive Sciences*, *9*(12), 556–559. https://doi.org/10.1016/j.tics.2005.10.010

Laureys, Steven, & Schiff, N. D. (2012). Coma and consciousness: Paradigms (re)framed by neuroimaging. *NeuroImage*, *61*(2), 478–491. https://doi.org/10.1016/j.neuroimage.2011.12.041

Lee, M., Baird, B., Gosseries, O., Nieminen, J. O., Boly, M., Postle, B. R., … Lee, S. W. (2019). Connectivity differences between consciousness and unconsciousness in non-rapid eye movement sleep: a TMS–EEG study. *Scientific Reports*, *9*(1), 1–9. https://doi.org/10.1038/s41598-019-41274-2

Lee, UnCheol, Kim, S., Noh, G. J., Choi, B. M., Hwang, E., & Mashour, G. A. (2009). The directionality and functional organization of frontoparietal connectivity during consciousness and anesthesia in humans. *Consciousness and Cognition*, *18*(4), 1069–1078. https://doi.org/10.1016/j.concog.2009.04.004

Lee, Uncheol, Ku, S., Noh, G., Baek, S., Choi, B., & Mashour, G. A. (2015). Disruption of Frontal-Parietal Communication by Ketamine, Propofol, and Sevoflurane. *Anesthesiology*, *118*(6), 1264–1275. https://doi.org/10.1097/ALN.0b013e31829103f5.Disruption

Leech, R., Braga, R., & Sharp, D. J. (2012). Echoes of the brain within the posterior cingulate cortex. *Journal of Neuroscience*, *32*(1), 215–222. https://doi.org/10.1523/JNEUROSCI.3689-11.2012

Litvak, V., Jafarian, A., Zeidman, P., Tibon, R., Henson, R. N., & Friston, K. (2019). There's no such thing as a "true" model: The challenge of assessing face validity. *Conference Proceedings - IEEE International Conference on Systems, Man and Cybernetics*, *2019-Octob*, 4403–4408. https://doi.org/10.1109/SMC.2019.8914255

Liu, X., Lauer, K., Ward, D., Li, S.-J., & Hudetz, A. (2013). Differential Effects of Deep Sedation with Propofol on the Specific and Nonspecific Thalamocortical Systems. *Anesthesiology*, *118*(1), 59–69. https://doi.org/10.1038/jid.2014.371

Luppi, A. I., Craig, M. M., Finoia, P., Williams, G. B., Naci, L., Menon, D. K., & Emmanuel, A. (2019). Consciousness-specific dynamic interactions of brain integration and functional diversity. *Nature Communications*, (Box 65). https://doi.org/10.1038/s41467-019-12658-9

Maksimow, A., Silfverhuth, M., Långsjö, J., Kaskinoro, K., Georgiadis, S., Jääskeläinen, S., & Scheinin, H. (2014). Directional connectivity between frontal and posterior brain regions is altered with increasing concentrations of propofol. *PLoS ONE*, *9*(11), 1–16. https://doi.org/10.1371/journal.pone.0113616

Mashour, G. A., Roelfsema, P., Changeux, J. P., & Dehaene, S. (2020). Conscious Processing and the Global Neuronal Workspace Hypothesis. *Neuron*, *105*(5), 776–798. https://doi.org/10.1016/j.neuron.2020.01.026

Moran, R. J., Kiebel, S. J., Stephan, K. E., Reilly, R. B., Daunizeau, J., & Friston, K. J. (2007). A neural mass model of spectral responses in electrophysiology. *NeuroImage*, *37*(3), 706–720. https://doi.org/10.1016/j.neuroimage.2007.05.032

Moran, R. J., Stephan, K. E., Seidenbecher, T., Pape, H. C., Dolan, R. J., & Friston, K. J. (2009). Dynamic causal models of steady-state responses. *NeuroImage*, *44*(3), 796–811. https://doi.org/10.1016/j.neuroimage.2008.09.048

Moran, R., Pinotsis, D. A., & Friston, K. (2013). Neural masses and fields in dynamic causal modelling. *Frontiers in Computational Neuroscience*, *7*(APR 2013), 1–12. https://doi.org/10.3389/fncom.2013.00057

Murphy, M., Bruno, M. A., Riedner, B. A., Boveroux, P., Noirhomme, Q., Landsness, E. C., … Boly, M. (2011). Propofol anesthesia and sleep: A high-density EEG study. *Sleep*, *34*(3). https://doi.org/10.1093/sleep/34.3.283

Nicolaou, N., Hourris, S., Alexandrou, P., & Georgiou, J. (2012). EEG-based automatic classification of "awake" versus "anesthetized" state in general anesthesia using granger causality. *PLoS ONE*, *7*(3). https://doi.org/10.1371/journal.pone.0033869

Raichle, M. E., & Snyder, A. Z. (2007). A default mode of brain function: A brief history of an evolving idea. *NeuroImage*, *37*(4), 1083–1090. https://doi.org/10.1016/j.neuroimage.2007.02.041

Ramsay, M. A. E., Savege, T. M., Simpson, B. R. J., & Goodwin, R. (1974). Hospital Topics Controlled Sedation with Alphaxalone-Alphadolone. *British Medical Journal*, *22*, 656–659.

Razi, A., & Friston, K. J. (2016). The Connected Brain: Causality, models, and intrinsic dynamics. *IEEE Signal Processing Magazine*, *33*(3), 14–55. https://doi.org/10.1109/MSP.2015.2482121

Razi, A., Seghier, M. L., Zhou, Y., McColgan, P., Zeidman, P., Park, H.-J., … Friston, K. J. (2017). Large-scale DCMs for resting-state fMRI. *Network Neuroscience*. https://doi.org/10.1162/NETN_a_00015

Rosa, M. J., Friston, K., & Penny, W. (2012). Post-hoc selection of dynamic causal models. *Journal of Neuroscience Methods*, *208*(1), 66–78.

https://doi.org/10.1016/j.jneumeth.2012.04.013

Salin, P. A., & Bullier, J. (1995). Corticocortical connections in the visual system: Structure and function. *Physiological Reviews*, *75*(1), 107–154. https://doi.org/10.1152/physrev.1995.75.1.107

Sanders, R. D., Banks, M. I., Darracq, M., Moran, R., Sleigh, J., Gosseries, O., … Boly, M. (2018). Propofol-induced unresponsiveness is associated with impaired feedforward connectivity in cortical hierarchy. *British Journal of Anaesthesia*, *121*(5), 1084–1096. https://doi.org/10.1016/j.bja.2018.07.006

Sarasso, S., Boly, M., Napolitani, M., Gosseries, O., Charland-Verville, V., Casarotto, S., … Massimini, M. (2015). Consciousness and complexity during unresponsiveness induced by propofol, xenon, and ketamine. *Current Biology*, *25*(23), 3099–3105. https://doi.org/10.1016/j.cub.2015.10.014

Schrouff, J., Perlbarg, V., Boly, M., Marrelec, G., Boveroux, P., Vanhaudenhuyse, A., … Benali, H. (2011). Brain functional integration decreases during propofol-induced loss of consciousness. *NeuroImage*, *57*(1), 198–205. https://doi.org/10.1016/j.neuroimage.2011.04.020

Sherman, S. M., & Guillery, R. W. (1998). On the actions that one nerve cell can have on another: Distinguishing “drivers” from “modulators.” *Proceedings of the National Academy of Sciences of the United States of America*, *95*(12), 7121–7126. https://doi.org/10.1073/pnas.95.12.7121

Siclari, F., Baird, B., Perogamvros, L., Bernardi, G., LaRocque, J. J., Riedner, B., … Tononi, G. (2017). The neural correlates of dreaming. *Nature Neuroscience*, *20*(6), 872–878. https://doi.org/10.1038/nn.4545

van den Heuvel, M. P., & Sporns, O. (2011). Rich-Club Organization of the Human Connectome. *Journal of Neuroscience*. https://doi.org/10.1523/jneurosci.3539-11.2011

van Wijk, B. C. M., Cagnan, H., Litvak, V., Kühn, A. A., & Friston, K. J. (2018). Generic dynamic causal modelling: An illustrative application to Parkinson's disease. *NeuroImage*, *181*(January), 818–830. https://doi.org/10.1016/j.neuroimage.2018.08.039

Vanhaudenhuyse, A., Noirhomme, Q., Tshibanda, L. J. F., Bruno, M. A., Boveroux, P., Schnakers, C., … Boly, M. (2010). Default network connectivity reflects the level of consciousness in non-communicative brain-damaged patients. *Brain*, *133*(1), 161–171. https://doi.org/10.1093/brain/awp313

White, N. S., & Alkire, M. T. (2003). Impaired thalamocortical connectivity in humans during general-anesthetic- induced unconsciousness. *NeuroImage*, *19*(2), 402–411. https://doi.org/10.1016/S1053-8119(03)00103-4

Wu, X., Zou, Q., Hu, J., Tang, W., Mao, Y., Gao, L., … Yang, Y. (2015). Intrinsic functional connectivity patterns predict consciousness level and recovery outcome in acquired brain injury. *Journal of Neuroscience*, *35*(37), 12932–12946. https://doi.org/10.1523/JNEUROSCI.0415-15.2015

Xia, M., Wang, J., & He, Y. (2013). BrainNet Viewer: A Network Visualization Tool for Human Brain Connectomics. *PLoS ONE, 8: e68910*.